Lana Virag[1], John S. Wilson[2],
Jay D. Humphrey[3,4], Igor Karšaj[1]

A Computational Model
of Biochemomechanical Effects
# of Intraluminal Thrombus and Roles
# of Risk Factors in the Evolution
# of Abdominal Aortic Aneurysms

[1]Faculty of Mechanical Engineering and Naval Architecture, University of Zagreb, Zagreb, Croatia

[2]Department of Radiology, Emory University, Atlanta, GA, USA

[3]Department of Biomedical Engineering, Yale University, and [4]Vascular Biology and Therapeutics Program, Yale School of Medicine, New Haven, CT, USA

Introduction

Abdominal aortic aneurysms (AAAs) are classically asymptotic localized enlargements of the infrarenal abdominal aorta that result primarily from an altered deposition and degradation of extracellular matrix. A catastrophic endpoint in the natural history of AAAs is rupture – an event with a high mortality rate. Unfortunately, current clinical capabilities for predicting rupture remain wanting, and clinical interventions continue to be based primarily on the maximum diameter or rate of enlargement of the lesion. Yet, many small lesions rupture while larger lesions do not [1,2], and many AAAs do not enlarge continuously. That is, radial enlargement of aneurysm often occurs via stepwise dilatations, with periods of stability alternating with periods of enlargement [3]. One possible reason for this variability in clinical outcomes is intraluminal thrombus (ILT). A large population-based study showed that all AAAs larger than 6 cm contain ILT, as do a majority of smaller lesions [4]. Such thrombi are typically layered structures that, unlike other blood clots, show few signs of healing. The portion of ILT closest to the flowing blood (i.e., the luminal layer) is characterized by an aggregation of activated platelets as well as the entrapment of erythrocytes (RBCs) and leukocytes within an evolving fibrin mesh that appears to remodel continuously. This layer is usually ~2 mm thick [5], which may be limited by the depth to which blood components can penetrate the fibrin mesh. Leukocytes within the luminal layer produce enzymes (e.g., matrix metalloproteinases (MMPs) and neutrophil elastase) that degrade the aortic wall or activate those that do (e.g., by activating urokinase plasminogen activator (uPA), which increases plasmin which activates latent MMPs). In contrast, the degradation of fibrin tends to outpace its deposition in the deeper layers of thick thrombi, often referred to as medial (middle) and abluminal (next to the aneurysmal wall). These deeper layers are also mostly devoid of cells [6]. The lack of platelets in these layers suggests little production of fibrin, hence degradation of fibrin likely dominates deposition within these layers. Whereas the biochemically active luminal layer can disrupt underlying wall structure, and thereby promote rupture of an AAA, most ILTs are much thicker than 2 mm. In these cases, the ILT may stress shield the wall mechanically [7] and may serve as a barrier to the diffusion of oxygen and proteases coming from the blood and luminal ILT. It is thus important to account for the complex and diverse biomechanical and biochemical roles of ILT when modelling AAA biomechanics [8].

Thrombus was ignored in AAA modelling until 1993, when Inzoli et al. [9] suggested that an ILT might mechanically shield the aortic wall and thereby decrease the peak wall stress and associated rupture risk. Despite overwhelming evidence that ILT is biochemically active [6,10], it has been either modelled as an inert, homogeneous material in static models that focus on the state of stress in the wall (e.g., [7]) or neglected in most G&R studies (e.g., [11,12]). Clearly, proteolysis could contribute to the chronic inflammation characteristic of AAAs. There is, therefore, a pressing need for greater understanding. The goal of this research was to develop a mathematically tractable, first generation G&R model of enlargement and possible rupture of thrombus-laden AAAs, including a framework for quantifying and predicting interrelationships between the biochemistry and biomechanics. Additionally, we examined potential differences in model predictions for physiological ranges of parameter values. We investigated the possible extent to which these parameters influence AAA evolution and to recognize the key features of the thrombus-laden model effects of commonly proposed factors that influence the risk of rupture. Thus, this study also provides some insight into possible roles of common risk factors on the natural history of AAAs.

Methods

We build on the model presented in [17], but for completeness we apply the salient equations here. We assumed that AAAs initiate from aged non-aneurysmal aortas and focused on an idealized cylindrical geometry to highlight emergent effects of differences in the values of the constitutive parameters. Although this 1D model thus considers mechanical changes and chemical diffusion in the radial direction alone, we submit that the associated predictions provide vital insight into the importance and interrelationship of many parameters in the model before including the additional complexities and significantly increased computational expenses of analyzing 3D geometries. Ultimately, careful attention and refinement, as these complex G&R models are developed, will increase the likelihood of an accurate understanding and simulation of patient-specific lesions, and can guide experimental efforts to understand, predict, and therapeutically address the roles of ILT in AAA progression.

Kinematics of AAA

We use the notation of Karšaj and Humphrey [10]. Briefly, individual constituents k deposited at a generic G&R time τ are incorporated within extant extracellular matrix with pre-stretch $\mathbf{G}^k(\tau)$, whereas the mapping of differential position vectors defined in individual natural configurations for each constituent produced at time τ to those in a current (deformed) mixture configuration at time s is captured by deformation gradient $\mathbf{F}_{n(\tau)}^k(s)$ (cf. Figure 1 in [10]). The right Cauchy-Green tensor $\mathbf{C}_{n(\tau)}^k(s)$ is thus ... Similarly, for the overall deformation gradient for the mixture $\mathbf{F}$, the associated right Cauchy-Green tensor is $\mathbf{C} = \mathbf{F}^{\mathrm{T}}\mathbf{F}$.

Kinetics of AAA

Following [17], elastin is not produced in maturity; hence, it can only degrade as the model progresses in time. In contrast, collagen and smooth muscle undergo turnover in the wall as does fibrin in the thrombus. Such turnover implies both degradation and deposition, the latter at production rate. Whereas deposition is constant at a basal production rate $\dot{m}_B^k$ during homeostasis, it may be altered in response to deviations in intramural stress from a homeostatic value $\left\|\mathbf{t}_h^k\right\|$ due to injury, disease, or inflammation. We let the current mass of each constituent k evolve as

$$M^k(s) = M^k(0)Q^k(s) + \int_0^s \dot{m}^k(\tau)q^k(s-\tau)\,\mathrm{d}\tau \quad (1)$$

where $q^k(s-\tau)$ is survival function defining the percentage of constituent produced at past time τ that re-

mains at current time s with a special case that $Q^k(s) = q^k(s-0)$. Given that $M^k(0)$ is the initial mass of constituent k, note that $M^e(s) = M^e(0)Q^e(s)$ for elastin since we assume no production in maturity.

We further let the survival function q^k depend on the rate-type removal parameter K_q^k, where

$$q^k(s-\tau) = \exp\left(-\int_\tau^s K_q^k(\tilde{\tau})\,\mathrm{d}\tilde{\tau}\right) \cdot Q^{k,e}(s), \quad (2)$$

with $Q^{k,e}(s) = 1$ for all constituents except muscle. To model anoikis of smooth muscle cells (i.e., apoptosis caused by a loss of attachment to surrounding matrix, including elastic fibers), the degradation of smooth muscle was linked to the degradation of elastin by $Q^{SMC,e}(s) = Q^e(s)$.

Intraluminal thrombus

Understanding of the spatially evolving deposition of thrombus remains wanting; however, many medical images of large AAAs suggest that the overall luminal diameter tends to be maintained. We therefore assumed that the luminal area remained constant throughout our simulations, meaning that additional ILT was deposited in every time step in which the lesion enlarged, often burying prior portions of the luminal layer which then became medial and abluminal layers (cf. [16] for the naming convention of ILTs. Moreover, based on experimental findings ([18]), we considered fibrin, fibrin degradation products (FDPs), erythrocytes (RBCs) and voids to be the most significant space-filling constituents of a layered ILT. Even though leukocytes, platelets and non-collagenous extracellular proteins were neglected as load-bearing constituents, they were nevertheless crucial for the biological activity of the thrombus.

Fibrin. During coagulation platelets release thrombin, which helps to convert soluble fibrinogen into fibrin that, in turn, polymerizes to form a cross-linked mesh. We modelled changes in the mass of fibrin similar to changes in wall constituents (eq. (1)), but assumed that the production rate of fibrin depended on the mass of platelets M_i^{plt} and decreased with increasing fibrin density ϕ_i^f through correlation parameter $K_{plt,\phi}^f$, such that

$$\dot{m}_i^f(\tau) = K_{plt,\phi}^f M_i^{plt}(\tau)\left(1 - \phi_i^f(\tau)\right) \quad (3)$$

Fibrin is dissolved by plasmin. Moreover, since fibrinolysis has been reported to be inversely proportional to the density of the fibrin mesh and its current stretch [19], we considered the mass removal rate-type parameter for fibrin of the form (cf.)

$$K_q^f(\tau) = k_q^f + w_q^f M_i^{pls}(\tau)\left(1 - \phi_i^f(\tau)\right)\big/\lambda_i(\tau), \quad (4)$$

where k_q^f is homeostatic value depending on the natural half-life of fibrin, M_i^{pls} is mass of plasmin, and λ_i is fibrin stretch; w_q^f is weighting function.

Cells and Platelets.

The majority of blood-derived cells within an ILT reside in the luminal layer ([5,20]), presumably because flowing blood can replenish and sustain cells only to a certain depth. Thus, we defined the boundary of the luminal layer by a depth beyond which cells could not be replenished, either because a critical fibrin mesh density $\phi_{crit}^{f,RBC}$ was reached or because a critical radius $r_{crit}(\tau)$ was attained. This critical radius was defined in each instant by a critical mass of fibrin M_{crit}^f, such that

$$\sum_{\eta}^{r_{crit}} M^f(r,\tau) = M_{crit}^f, \qquad (5)$$

where M_i^f is mass of fibrin in layer i. The quantity of blood-borne cells in the luminal layer depended on their luminal concentration (e.g. M_l^{plt} for platelets). We assumed the first order decay process for cells that became buried in the medial layer (with a half-life $\tau_{1/2}^{plt}$ of 7 to 11 days for platelets and $\tau_{1/2}^{RBC} = 120$ days for erythrocytes). In summary, the mass of platelets (and similarly for leukocytes, primarily neutrophils, M_i^N) was calculated as

$$M_i^{plt}(\tau) = \begin{cases} M_l^{plt}(\tau) & \text{except if} \\ M_l^{plt}(\tau_{crit}^{i,1}) \cdot e^{-K_q^{plt}(\tau - \tau_{crit}^{i,1})} & r_i(\tau) \geq r_{crit}(\tau) \\ M_l^{plt}(\tau_{crit}^{i,2}) \cdot e^{-K_q^{plt}(\tau - \tau_{crit}^{i,2})} & \phi_j^f(\tau) \geq \phi_{crit}^{f,plt}, \ \forall j \geq i \end{cases} \qquad (6)$$

where $\tau_{crit}^{i,1}$ is the time at which a critical mass of fibrin (i.e., r_{crit}) was achieved, thus transitioning the layer from luminal to medial. Similarly, $\tau_{crit}^{i,2}$ represents the time at which the limit of the luminal layer was achieved by reaching the critical mass fraction of fibrin (i.e., mesh density). Leukocytes were assumed not to contribute significantly to the volume of the ILT; nonetheless, their presence is important for biochemical activity (e.g., production of plasmin, MMPs or other elastases).The distribution of erythrocytes within the ILT was defined similarly, with the exception of using a mass fraction necessary to calculate the overall stored energy of ILT instead of the mass.

Plasmin, EDPs, and neovascularization.

Conversion of plasminogen to plasmin is a complex process catalyzed by multiple enzymes, including a key step by either tissue plasminogen activator (tPA, found on endothelial cells) or urokinase plasminogen activator (uPA, coming mainly from the blood stream via mesenchymal and inflammatory cells). Conversely, activation may be inhibited by plasmin activation inhibitor (PAI-1) and alpha-2 antiplasmin. For this simplified model, we sought to capture phenomenologically the overall increase in activated plasmin and to model its diffusion from two primary sources: the leukocyte-rich luminal layer of the ILT and the inflamed aneurysmal wall (to which leukocytes invade via the vasa vasorum). This increased production of plasmin within the wall is consistent with immunohistological reports [21]. The mass of activated plasmin M_i^{pls} that degrades fibrin is given as

$$M_i^{pls}(\tau) = K_N^{pls} M_i^N(\tau) + \underbrace{M_{wall}^{pls}(\tau) - \sum_{j=1}^{i} K_f^{pls} M_j^f(\tau)}_{\geq 0}, \quad (7)$$

where K_N^{pls} is correlation factor between plasmin and neutrophils in the thrombus, K_f^{pls} is the amount of plasmin consumed per unit of fibrin, and $M_{wall}^{pls}(\tau)$ is the mass of plasmin in the wall, calculated as $M_{wall}^{pls}(\tau) = K_{EDP}^{pls} M_{tot}^{EDP}(\tau) + K_{VV}^{pls} A_{tot}^{VV}(\tau)$. We assumed that the plasmin generated within the wall largely depends on the total mass of elastin degradation products M_{tot}^{EDP}, which are chemo-attractants for inflammatory cells and stimulate neovascularization of the wall (i.e., increase the area of vasa vasorum A_{tot}^{VV}, [22]). Correlations between plasmin and EDPs/vasa vasorum were accounted for by K_{EDP}^{pls} and K_{VV}^{pls}, respectively. The production rate of EDPs directly depended on the amount of elastin degraded per time step, while their degradation was modelled as the first-order decay with constant half-life. The total mass of EDPs can then be calculated by eq. (1).

Due to the controversial influence of hypoxia on neovascularisation, the studies that showed EDPs alone promote neovascularization [22], we modelled the development of vasa vasorum solely as a function of the mass of EDPs, such that

$$A_{tot}^{VV}(s) = A_0^{VV} + \int_0^s K_{EDP}^{VV} M_{tot}^{EDP} \, d\tau, \qquad (8)$$

where A_0^{VV} is the area of vasa vasorum in healthy aorta, and K_{EDP}^{VV} is the correlation factor that relates vasa vasorum growth per unit of EDPs per unit time.

Fibrin degradation products and voids.

The luminal layer contains entrapped erythrocytes within a thick fibrin mesh. Once the luminal layer is buried deeper within the thrombus, erythrocytes cannot be replenished. Likewise, the amount of platelets necessary for fibrin deposition decreases steeply, thus allowing degradation to outpace deposition. Dissolution of fibrin and apoptosis of red blood cells can leave small interconnected channels ("voids" or "canaliculi") throughout

the ILT [5]. We assumed that degrading fibrin was converted partly into fibrin degradation products (FDPs) and partly into canaliculi (as fibrin was removed by macrophages) in a 7:3 ratio.

Biochemical interaction of ILT and aneurysmal wall

Effects of the proteolytically active luminal layer were integrated via additional terms in the mass removal rate-type parameter K_q^k in eq. (2). For example, the elastin in normally aging aorta depends solely on its natural half-life $\tau_{1/2}$ on the order of forty to fifty years: $K^e = k_q^e = \ln(2)/\tau_{1/2}^e$. Increased degradation of elastin in an aneurysm due to inflammation was incorporated via an additional term,

$$K_q^e(\tau) = k_q^e + w_{q,elas}^e M^{elas}(r,\tau), \qquad (9)$$

where elastases, M^{elas}, was modulated by a weighting factor $w_{q,elas}^e$.

Correspondingly for collagen, we let (cf. [10])

$$K_q^c(\tau) = \left(\partial W^c / \partial \mathbf{F}_{n(\tau)}^c\right) / \left(\partial W^c / \partial \mathbf{F}_{n(0)}^c\right) k_q^c + \\ + w_{q,MMP}^c M^{MMP}(r,\tau) \qquad (10)$$

where the collagen mass removal parameter K_q^c depends on the ratio of the current ($\partial W^c / \partial \mathbf{F}_{n(\tau)}^c$) to the homeostatic ($\partial W^c / \partial \mathbf{F}_{n(0)}^c$) tension, and k_q^c is the rate-type removal parameter associated with homeostatic half-life; the additional terms relate to the distribution of active MMPs (i.e., collagenases). Similar to plasmin, MMPs may arise from two sources: luminal layer in ILT or vasa vasorum in the aortic wall. The first approximation, quasi-static transport, was determined easily from the diffusion equation, $\frac{\partial M^{elas}}{\partial t} = \nabla \cdot \left[D \nabla M^{elas} \right]$, where D is the diffusion coefficient that can be estimated based on the available data of the radial distribution of proteases [15,20]. We defined the available elastase/MMPs from the luminal layer, $K_N^{elas} M_{tot}^N$ (or $K_N^{MMP} M_{tot}^N$ for MMPs), where $K_N^{elas/MMP}$ described how much elastase/MMP was produced per unit of leukocytes per time step, as a point source centered at radius r_L, where

$$r_L(s) = \frac{1}{M_{tot}^N(s)} \sum_i M_i^N(s) r_i(s), \qquad (11)$$

similar to the center of mass. The concentration of elastase/MMPs available at the outer radius depended on the area of vasa vasorum and number of inflammatory cells: $K_{WBC}^{elas} M_{tot}^{WBC}(s) + K_{VV}^{elas} A_{tot}^{VV}(s)$. Thus, by solving the diffusion equation, the overall distribution of proteases was:

$$M^k(r,s) = \\ \frac{K_N^k M_{tot}^N(s) - K_{WBC}^k M_{tot}^{WBC}(s) - K_{VV}^k A_{tot}^{VV}(s)}{\ln(r_L(s)/r_o)} \ln(\frac{r(s)}{r_o}), \quad (12) \\ + K_N^k M_{tot}^N(s)$$

where k indicates elastases or collagenases. Mass of inflammatory cells in the wall, M_{tot}^{WBC}, was modelled similar to with degradation depending on cellular half-life, and production $\dot{m}_{tot}^{WBC}$ increasing with the growth of EPD mass and vasa vasorum, such that

$$\dot{m}_{tot}^{WBC}(\tau) = K_{EDP,VV}^{WBC} \left(\frac{A_{tot}^{VV}(\tau)}{A_0^{VV}} \right)^\alpha M_{tot}^{EDP}(\tau), \quad (13)$$

where $K_{EDP,VV}^{WBC}$ is the correlation factor that relates proliferation of white blood cells with EDPs and neovascularisation, and α is power parameter.

Stress analysis

The Cauchy stress within the aortic wall was calculated as a constrained mixture,

$$\mathbf{t} = \frac{2}{\det(\mathbf{F})} \mathbf{F} \frac{\partial W}{\partial \mathbf{C}} \mathbf{F}^T + t^{active} \mathbf{e}_\theta \otimes \mathbf{e}_\theta, \qquad (14)$$

with $W = \sum_k W^k$ the overall stored energy function, and t^{active} the active stress contribution from circumferentially oriented smooth muscle contractility. Similar to Valentín et al. [23], phenotypic transitioning of smooth muscle cells from a contractile to synthetic state is considered by allowing the decreasing maximal active stress T_m such that $T_m(s) = T_m(0) \cdot \left(\beta_m + (1 - \beta_m) Q_e(s) \right)$.

By noting that fibers deposited into extant matrix at different times have different deformation gradients, the total stored energy of the constituent is the combination of the unique stored energies of each fiber, namely

$$W^k(s) = \frac{M^k(0)}{\sum_k M^k(s)} \hat{W}^k \left(\mathbf{C}_{n(0)}^k(s) \right) Q^k(s) \\ + \int_0^s \frac{\dot{m}^k(\tau)}{\sum_k M^k(s)} \hat{W}^k \left(\mathbf{C}_{n(\tau)}^k(s) \right) q^k(s-\tau) \, d\tau \qquad (15)$$

For the inherent stored-energy form of each type of the constituent ($\hat{W}^k$), isotropic elastin is modelled as neo-Hookean, while collagen and smooth muscle are modelled as fiber-like with an exponential constitutive response in tension but no compressive stiffness, as in [17].

Mechanically, ILT can bear stress and possibly reduce peak wall stress. Cauchy stress in the ILT was modelled using the stored energy function for an isotropic fibrin

mesh based on [18], and the neo-Hookean strain energy function was used for the FDPs.

Prediction of Aaa Progression Based on Risk Factors

The ultimate goal of computational modelling of aneurysmal G&R is to help clinicians predict rupture risk. Although multiple potential risk factors of AAA rupture have been suggested [24], we consider herein a few key factors within the limitations of our model. Note that rupture herein was defined as any normal component of wall stress reaching 460 kPa [25].

Smoking

Smoking has been linked to multiple vascular diseases. Among many other effects, it elevates oxidative stress, injures arterial endothelium, and promotes atherogenesis [26]. It increases the oxidation of low density lipoproteins, which promotes monocyte adhesion and migration into the subintimal space and thereby increases recruitment of inflammatory cells in the vascular wall [27]. Smoking also increases the concentration of plasma fibrinogen and alters the activity of platelets, thus potentiating thrombosis along dysfunctional endothelium [27]. Finally, it correlates strongly with increased aortic blood pressure, heart rate, and arterial stiffness [28]. It has been suggested further that smoking-induced arterial stiffening is isotropic, as reflected by a consistent increase in an elastin-associated parameter [29].

Many studies associate smoking with larger AAAs [3,30] and expansion rates [31]. Some studies suggest that cessation of smoking may inhibit aneurysmal expansion, even though two years of cessation does not reduce arterial stiffness [32]; indeed, it can take up to a decade to reduce stiffness to the level of never-smokers [33]. Similarly, five years of abstinence can reduce fibrinogen concentrations to the range of never-smokers [34].

Motivated by these studies, we investigated the natural histories of aneurysms in simulated smokers, ex-smokers, and those who had never smoked. Smoking was modelled by an increased elastin stiffness, inflammation, and platelet activity. Endothelial and smooth muscle cell dysfunctions are characteristic of aneurysms independent of smoking and were implicitly included in the model for both smokers and non-smokers. For smoking cessation, we assumed a linear decrease over 10 years in the smoking-induced increase in elastin stiffness and linear decrease over 5 years in inflammation to the never-smoker level. All other G&R parameters were identical among the groups.

After 20 years the simulated AAA diameter was greater for smokers (5.39 cm) than non-smokers (4.40 cm) with an associated average increase in the dilatation rate of 0.0495 cm/year compared with non-smokers (Figure 1). These results are consistent with clinical observations. Bhak et al. [30] reported that smoking was associated with a 0.05±0.01 cm/year increase in the linear expansion rate. A comparison of AAAs in smokers and non-smokers to aneurysms simulated with only increases in elastin stiffness or increases in both elastin stiffness and inflammation suggest that inflammation played the greatest role early in aneurysmal progression, though increased stiffness alone could lead to large aneurysms over time (Figure 1). Increased plasma fibrinogen concentration and platelet activity (present in the smoker group but not in the group with only elastin stiffness and inflammation) did not have a significant influence on AAA evolution (dotted vs. dashed line). There was only a slight decrease in the AAA size due to the increased production of fibrin through higher platelet activity, which resulted in a slightly stiffer, thinner luminal layer. Note that this does not mean that an increased platelet activity could potentially stabilize AAAs since platelets are chemotactic for neutrophils and monocytes [35] and can cause higher inflammation and expansion rates.

Changes in rates of dilatation after smoking cessation have not been studied well, though there is some evidence of a slow (perhaps non-significant) decline in dilatation and risk of aneurysm development after cessation of smoking [36]. Thus, consistent with general public health guidelines, the immediate cessation of smoking is recommended, preferably before AAA development.
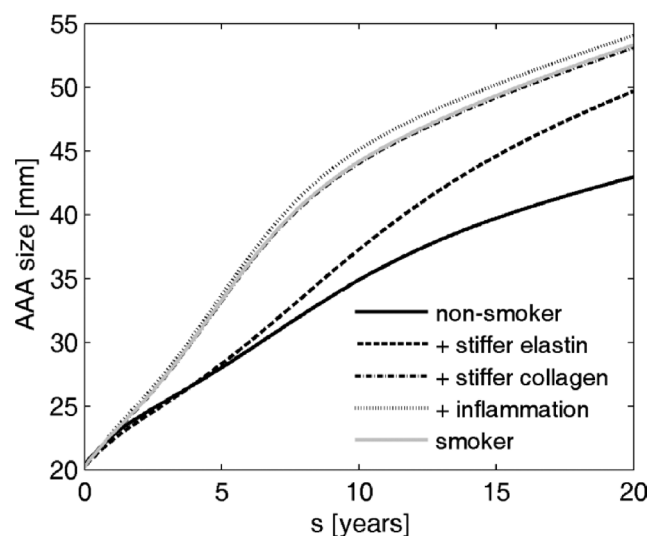

Fig. 1. Simulated evolution of an AAA in a non-smoker (solid line), in cases of increased elastin stiffness (dash-dotted line), increased elastin stiffness plus elevated inflammation (dotted line), and increased elastin stiffness, higher inflammation, and increased platelet activity (dashed line) – that is, full effects of smoking.

Aneurysm stabilization factors

Numerous studies have proposed various anti-inflammatory drugs for reducing or arresting the enlargement of AAAs, some of which act directly on MMPs [37,38] while others reduce inflammation indirectly (e.g., by platelet inhibitors [39,40] or immunosuppressive agents [41]). Another study in mice [37] suggested the importance of preserving medial elastin in order to attenuate aneurysmal dilatation. Although animal models have yielded conflicting results on roles of MMP inhibition or altering transforming growth factor TGF-β signaling on AAA expansion, some results have been encouraging. Nevertheless, non-specific MMP inhibition has not been found to reduce aneurysm progression in human patients [42]. Clearly, there is a need for increased understanding of the biochemical mechanisms of aneurysm formation and evolution.

Figure 2 shows that our thrombus-laden aneurysm model supports results from [37], where the inhibition of elastase (i.e., a slower degradation of elastin) helped to prevent rupture, and to some extent lead towards stabilizing the aneurysm, independent of collagen stiffness.

Other studies focused on the specific or non-specific inhibition of collagenases, which in most animal models led to stabilization. Similarly, the current model suggests that high rates of collagen degradation can lead to a progressive enlargement (solid line in Figure 3), though reduced inflammation could perhaps prevent a rupture (dashed line in Figure 3). Thus, the current results suggest that degradation rates of both elastin and collagen (i.e., concentrations of proteases, controlled for example by parameters $w^e_{q,elas}$ and $w^{MMP}_{q,elas}$ in eq. (9)) may strongly influence aneurysmal progression.

Gender and age

Gender differences have been identified in cardiovascular aging and in the evolution, management, and response to treatment for many cardiovascular diseases, including AAAs [43]. For example, females have stiffer large arteries in pre-puberty, but more compliant ones in post-puberty [44]. Additionally, age-associated endothelial function declines in men years before women [45]. These findings, among many others, could contribute to the increased prevalence of AAAs in men compared to women [46]. Yet, males have a 3-4 times lower risk of rupture than females [43], possibly due to higher strength of the AAA wall [47]. Similarly, noting that males have stiffer arteries on average [48], previous G&R models suggested that increased material stiffness of collagen decreases the likelihood of rupture.

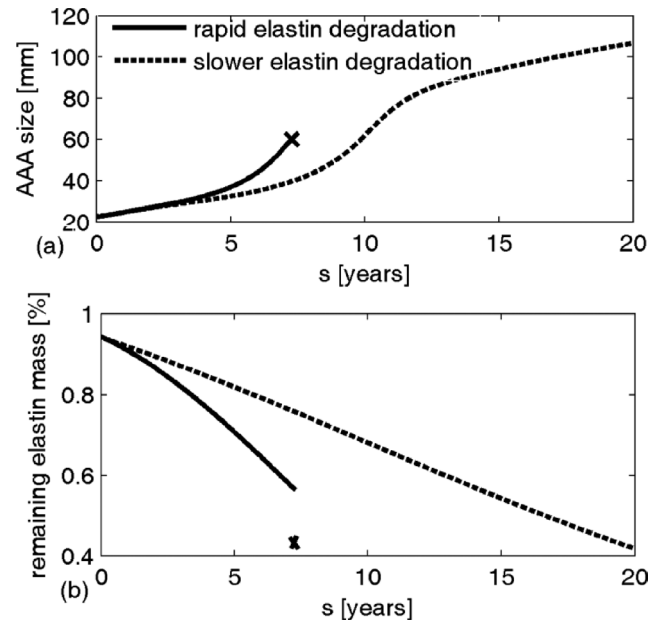Beyond biological sex, age may also play a role in AAA progression. Wilson et al. [12] demonstrated in a G&R

Fig. 2. Simulated AAA evolution (a) and corresponding degradation of elastin (b) in cases of rapid versus slow elastin degradation. Note that the aneurysm was initiated by degrading 5% of elastin. Rupture is denoted by "x".
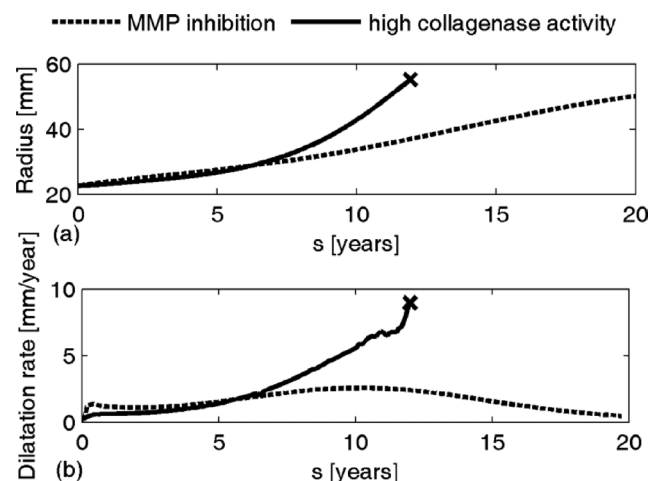

Fig. 3. Simulated AAA evolution (a) and associated dilatation rates (b) for different rates of collagen degradation in case of stiffening of collagen. "x" denotes rupture.

model that initial aortic properties may strongly influence AAA progression. Such properties are likely dependent on a patient's biological age (i.e., genetics, smoking status, comorbidities, exercise, etc.) as opposed to chronological age. For example, the observation that females who undergo open surgical repair for AAA are significantly older compared to males [48] may be reflective of their "younger" biological status as aforementioned in their later decline of endothelial function. Therefore, we explored differences in AAA expansion in males and females. The gender difference was modelled by different collagen stiffness (collagen in males stiffens, whereas in females collagen stiffness remains constant) and different initial structure of aorta. Formation of aneu-

rysm at a younger age, possibly typical for men, was taken into account by higher amounts of elastin (33.6% in younger vs. 27.4% in older), and a thinner intima (4% vs. 16%). Additionally, elastin in younger patients is less pre-stretched compared to older (1.3 in younger vs. 1.4 in older).

Similar to the results for the development of hypertension before AAA aneurysms developed on a stiffer aortic wall led to smaller expansion rates, with less likelihood of rupture (Figure 4).With regards to age, a younger aortic wall was more compliant and underwent larger deformations (whether ruptured or unruptured). It also had higher amounts of elastin, whose preservation is suggested to prevent rupture (see section 3.2). Therefore, the age at which an aneurysm develops might have an important impact on AAA evolution and might be an additional factor contributing to a high rupture risk in females.
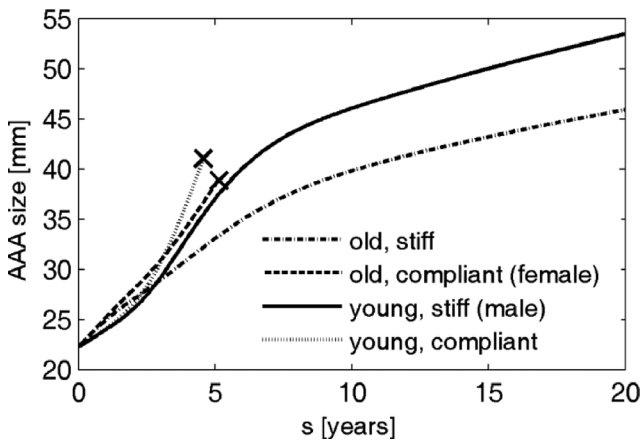

Fig. 4. Simulated evolution of AAAs for males and females of varying age. "x" denotes rupture.

Hypertension

Hypertension has been suggested as a key factor in driving AAA expansion [30] and rupture-risk, particularly in aneurysms smaller than 5.5 cm [49]. Hypertension leads to progressive changes in vascular structure, stiffness, thickness, radial dilatation and axial lengthening [50], all of which are G&R responses. To evaluate the effect of hypertension on AAA progression, we considered two cases: patients who were hypertensive before development of an AAA and patients who developed hypertension during the progression of the lesion. In the former case, computational results suggested that aneurysms originating from a hypertensive wall (simulated starting from healthy, non-hypertensive aorta) tend to rupture or stabilize at smaller sizes (Figure 5 (a)), depending on the properties of collagen.

When hypertension developed during aneurysmal progression, the luminal radius changed under the altered load. Thus, the luminal area was allowed to dilate to the size of an equivalent hypertensive, non-aneurysmal
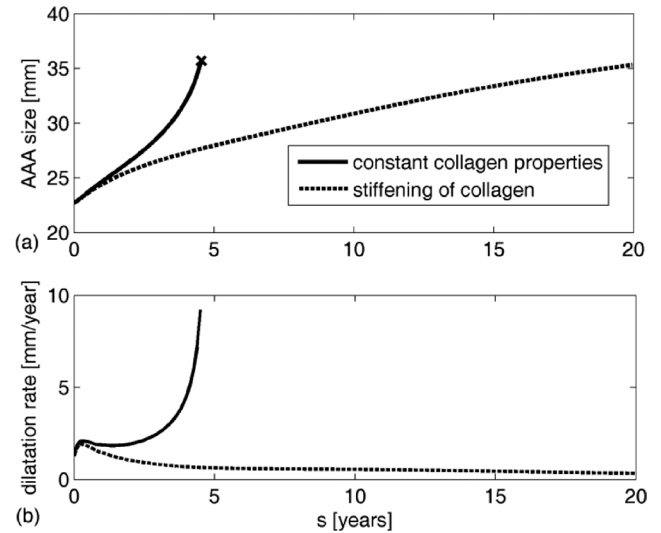

Fig. 5. Evolution of AAA diameter (a) and expansion rate (b) from a hypertensive aorta. Solid lines represent dilatation for constant collagen material properties; dashed lines represent enlargement during collagen stiffening.

aorta. We considered three stages of hypertension [51] defined as increases in mean blood pressure of 40% (36 mmHg), 60% (54 mmHg), and 80% (72 mmHg).

As expected, a greater increase in blood pressure resulted in a larger diameter (Figure 6). The average increase in expansion rate of a hypertensive aneurysm over 15 years was 0.0235, 0.0228 and 0.0221 cm/year per 10 mmHg increase for stages 1, 2 and 3, respectively. This is in good accordance with clinical observations of 0.02 ±0.01 cm/year per 10 mmHg [30]. Interestingly, computational results also suggested that a later development of hypertension is more likely to lead to rupture even though earlier hypertension leads to larger AAAs (Figure 7). This finding highlights the importance of G&R compensation as it is not strictly the diameter that determines rupture but the failure of a system to adequately compensate to a perturbation (i.e., dilatation need not mean decompensation). In this case, a relatively healthier wall
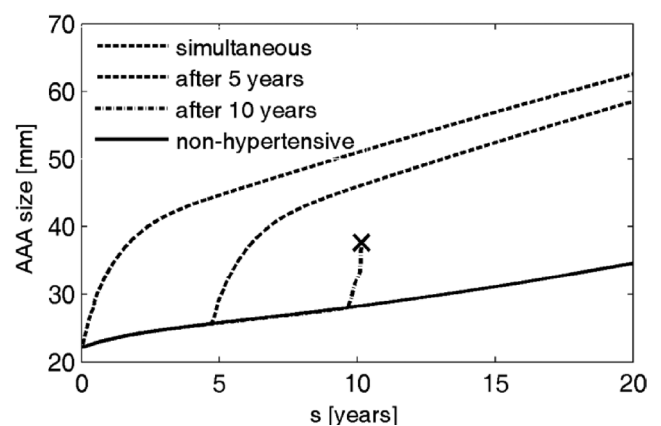

Fig. 6. Evolution of AAAs arising from a healthy aorta after retaining normal blood pressure (solid), or spontaneously developing stage 1 (dashed), stage 2 (dash-dotted), or stage 3 hypertension (dotted).
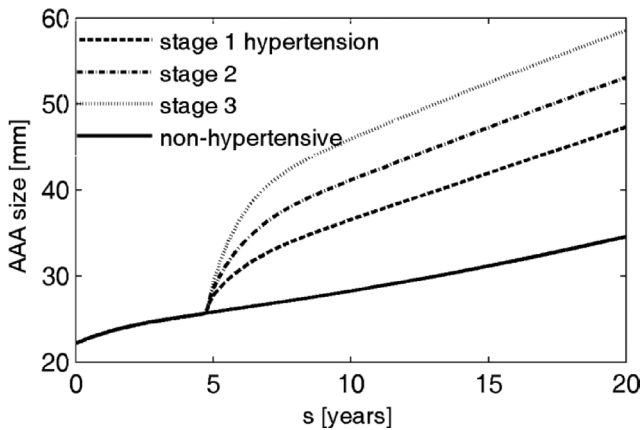
Fig. 7. Evolution of AAAs from an initially normotensive following development of stage 3 hypertension at different times during AAA progression. "x" denotes rupture.

(i.e., earlier in AAA development) was better able to compensate for higher blood pressure than was the wall exposed to the same pressure after being more extensively damaged as the AAA progressed.

Thickness of intraluminal thrombus

Another potential risk factor that has garnered increased attention is the size of the ILT. Different measures of ILT size, including thrombus thickness [52], volume [53], and relative cross-sectional area [3] were correlated with rapid expansion or rupture. Yet other studies suggest that ILT volume is the same in ruptured and intact AAAs [54], and case reports of unruptured giant thrombus-laden aneurysms (e.g., 25 cm in [55]) were described. Because of the cylindrical geometry used herein, it was not possible to consider whether rupture risk is linked to ILT volume or area. Nevertheless, we note that the distribution of proteases (M^{elas} for elastase and M^{MMP} for collagenase) in this 1D model depends on both the available proteases from each source (luminal layer of the ILT and vasa vasorum in the aortic wall) and the distance between the two sources; hence, it is related directly to ILT thickness.

The amount of available proteases in the luminal layer varies significantly among patients, from virtually non-existent to very high (e.g., see measured MMP-9 activity in both thrombus and wall specimens from 35 patients in Figure 2 in [21]). Thus, we investigated the possible evolution of an AAA for different amounts of protease activity in the ILT (by increasing $K_N^k M_{tot}^N(s)$ in eq. (12)). Figure 8 shows differences in predicted AAA enlargement in cases wherein the ILT and vasa vasorum have equal proteolytic activity ((a)-(c)) or the ILT is an order of magnitude more active ((d)-(f)). In the latter case, the proteolytic activity in the wall increased sharply as long as the luminal layer was directly attached to the aneurysmal wall (i.e., while the solid and dashed lines in

Figure 8 (a) coincide), thus resulting in rapid expansion of the aneurysm. As the less proteolytically active deeper layers form and act as a barrier to protease diffusion, proteolytic activity decreased abruptly and the expansion rate declined (Figure 8 (c) and (f)).

Interestingly, higher activity within the luminal layer led to a greater reduction in the expansion rate once the luminal layer was displaced from the wall, even causing a temporary near cessation of expansion (Figure 8 (f)). Several studies (e.g. [2]) report that the majority of AAAs dilate discontinuously with periods of expansion alternating with periods of quiescence. Though the exact cause of this phenomenon has not been determined, the current results suggest that ILT, specifically altering the proximity of the biologically active luminal layer from the wall, may directly influence expansion rates and thus play a role in determining clinical outcomes. Although only one cycle of expansion and arrest is allowed in this axisymmetric cylindrical geometry, expanding this model to 3D patient-specific geometries will allow further testing of the relationship of ILT, discontinuous expansion, and patient-specific outcomes by exploring more complex expansion patterns due to eccentric deposition of thrombus (i.e. where one portion of the ILT remains thinner than the other), non-continuous deposition of thrombus, local bulging and multiple regions where the wall is adjacent to thin thrombus throughout AAA development.

For both levels of activity within the luminal layer, a second peak of MMP activity and expansion rate was observed due to an increase in proteases from a developing vasa vasorum driven (in this model) by elastin degradation products. Interestingly, this second MMP peak is greater in the model with a lower luminal activity even though the expansion rate is lower.

As expected, note from Figure 8 (a) and (d) that the simulated AAA was larger after 20 years in the case of a high proteolytic activity (5.5 cm vs. 4.5 cm in outer diameter). Yet, there is no indication that thrombus thickness is directly responsible for AAA rupture as seen from simulations in previous sections where ruptures occurred in both small and large aneurysms, and some large aneurysms (11cm) remained stable. Further finite element analyses are warranted for confirmation, but we do not expect ILT thickness or other simple measures of ILT size to enable rupture predictions directly.

Conclusion

The field of computational biomechanics is increasingly used to investigate complex processes in vascular health and disease. Prior G&R models of aortic aneurysms (cf. [11,12]) have provided considerable insight that complement histopathological studies and clinical observations,
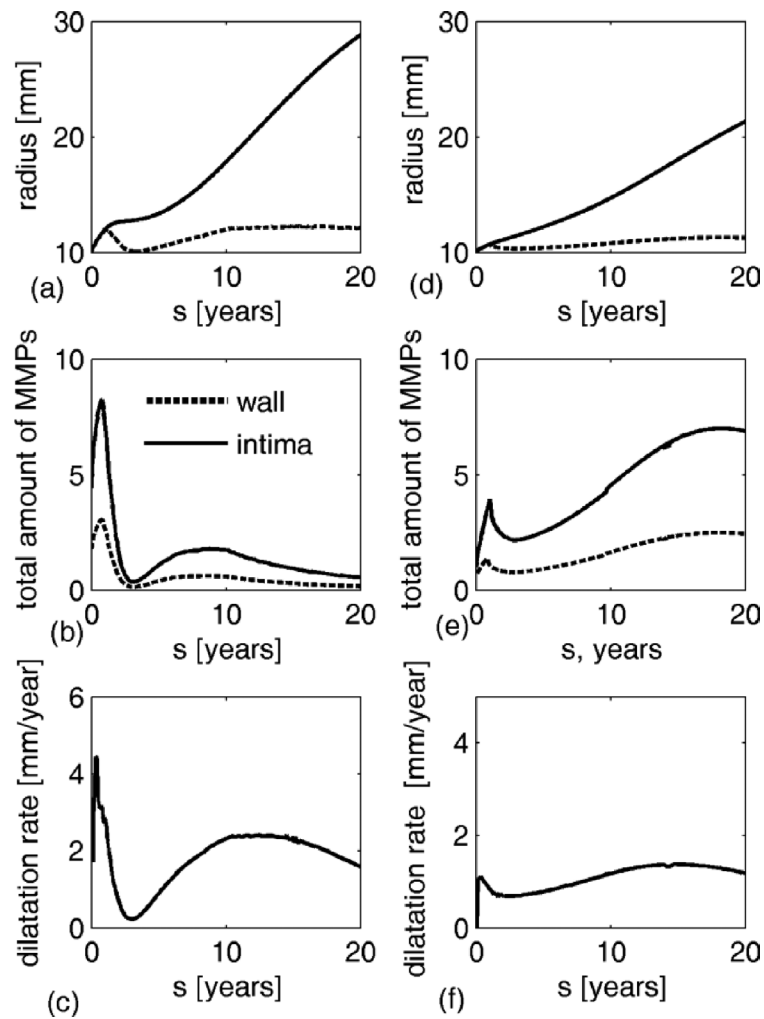
Fig. 8. Evolution of radius, MMPs, and expansion rate for AAAs with low proteolytic activity in the luminal layer of ILT (a-c) versus high proteolytic activity (d-f). (a,d) Evolution of radius at the ILT/wall interface (solid line) and luminal layer/wall or medial layer interface (dashed line). (b,e) Evolution of the normalized total amount of MMPs in the wall (solid line) and intima (dashed line). (c.f) Evolution of expansion rate.

but have heretofore failed to include the biochemomechanical effects of intraluminal thrombus on the aneurysmal wall. We consider these effects to be fundamental to the evolution of this disease and therefore for predicting clinical outcomes related to AAA enlargement and rupture. The current model was developed using a cylindrical geometry in order to focus on the importance of different constitutive assumptions and ranges of parameter values before introducing complex geometric effects that arise with local bulging. Clearly, such effects require investigation in future studies; nevertheless, this initial simplification yielded new insights into both the important roles that ILT may play during the evolution of aneurysms and the potential roles of diverse risk and stabilization factors.

While it appears that stiffening of collagen may increase the chances of stabilizing an aneurysm, it might not be sufficient. Inhibition of elastase activity could be important in preventing rupture, particularly since elastin degradation products can drive further inflammation and matrix loss. The simulations further suggested that an

ILT can significantly influence AAA expansion and rupture risk. Notably, high proteolytic activity in the luminal layer of the thrombus may increase expansion rate and rupture risk when in close proximity to the remodeling wall (i.e., a thin thrombus), and the evolving ILT may contribute to clinically observed discontinuous expansion patterns. We conclude, therefore, that ILT should not be neglected in future experimental and computational models.

Despite the geometric limitation and inability to capture complexities such as eccentric thrombus or local non-axisymmetric bulging of the lesion, the basic results were largely consistent with clinical observations, intuition, and previous computational G&R models having more complex geometries but without thrombus. Simulations yielded average rates of expansion of around 2 mm/year, whereas rapid expansion (1-2 cm/year) led to rupture. Smoking increased expansion rates by ~0.050 cm/year, and hypertension increased expansion by ~0.022 cm/year per 10 mmHg, both of which are clinically observed [33]. The model confirms and offers ad-

ditional support to female gender, smoking, and hypertension being factors that increase rupture-risk.

Given the understanding gleaned from this simple geometric model, there is now a need to move toward more complex (axisymmetric, non-axisymmetric and patient-specific) geometries with axially and circumferentially variable thrombus thickness (i.e., shoulder regions and eccentric thrombus). In order to assess the effects of spatially heterogeneous weakening in regions with thin thrombus and mechanical shielding in regions with thicker thrombus. Indeed, full fluid-solid-growth models would be ideal [58], as ILT formation and growth are strongly influenced by hemodynamics. In conclusion, we suggest that a careful consideration of the mechanical, chemical, and biological influences of proteolytically active, multi-layered intraluminal thrombus on AAA development will be required to maximize the potential for identifying and ameliorating rupture-risk factors (or, equally important, promoting stabilization factors), providing patient-specific diagnostics and interventional planning, and ultimately improving clinical outcomes.

References:

[1] Darling, R. C., Messina, C. R., Brewster, D. C. & Ottinger, L. W. 1977 Autopsy study of unoperated abdominal aortic aneurysms. The case for early resection. *Circulation* **56**, II161-4.

[2] Choksy, S. A., Wilmink, A. B. & Quick, C. R. 1999 Ruptured abdominal aortic aneurysm in the Huntingdon district: a 10-year experience. *Ann. R. Coll. Surg. Engl.* **81**, 27–31.

[3] Kurvers, H. et al. 2004 Discontinuous, staccato growth of abdominal aortic aneurysms. *J. Am. Coll. Surg.* **199**, 709–15.

[4] Behr-Rasmussen, C., Grøndal, N., Bramsen, M. B., Thomsen, M. D. & Lindholt, J. S. 2014 Mural thrombus and the progression of abdominal aortic aneurysms: a large population-based prospective cohort study. *Eur. J. Vasc. Endovasc. Surg.* **48**, 301–7.

[5] VandeGeest, J. P., Sacks, M. S. & Vorp, D. A. 2006 A planar biaxial constitutive relation for the luminal layer of intra-luminal thrombus in abdominal aortic aneurysms. *J. Biomech.* **39**, 2347–54.

[6] Houard, X. et al. 2007 Topology of the fibrinolytic system within the mural thrombus of human abdominal aortic aneurysms. *J. Pathol.* **212**, 20–28.

[7] Wang, D. H. J., Makaroun, M. S., Webster, M. W. & Vorp, D. A. 2002 Effect of intraluminal thrombus on wall stress in patient-specific models of abdominal aortic aneurysm. *J. Vasc. Surg.* **36**, 598–604.

[8] Humphrey, J. D. & Holzapfel, G. A. 2012 Mechanics, mechanobiology, and modeling of human abdominal aorta and aneurysms. *J. Biomech.* **45**, 805–14.

[9] Inzoli, F., Boschetti, F., Zappa, M., Longo, T. & Fumero, R. 1993 Biomechanical factors in abdominal aortic aneurysm rupture. *Eur. J. Vasc. Surg.* **7**, 667–74.

[10] Fontaine, V. et al. 2004 Role of leukocyte elastase in preventing cellular re-colonization of the mural thrombus. *Am. J. Pathol.* **164**, 2077–87.

[11] Watton, P. N. & Hill, N. A. 2009 Evolving mechanical properties of a model of abdominal aortic aneurysm. *Biomech. Model. Mechanobiol.* **8**, 25–42.

[12] Wilson, J. S., Baek, S. & Humphrey, J. D. 2012 Importance of initial aortic properties on the evolving regional anisotropy, stiffness and wall thickness of human abdominal aortic aneurysms. *J. R. Soc. Interface* **9**, 2047–58.

[13] Karšaj, I. & Humphrey, J. D. 2012 A multilayered wall model of arterial growth and remodeling. *Mech. Mater.* **44**, 110–119.

[14] Virag, L., Wilson, J. S., Humphrey, J. D. & Karšaj, I. 2015 A computational model of biochemomechanical effects of intraluminal thrombus on the enlargement of abdominal aortic aneurysms. *Ann. Biomed. Eng.* **43**, 2852–2867.

[15] Zambrano, B. A., Gharahi, H., Lim, C., Jaberi, F. A., Choi, J., Lee, W. & Baek, S. 2015 Association of intraluminal thrombus, hemodynamic forces, and abdominal aortic aneurysm expansion using longitudinal CT images. *Ann. Biomed. Eng.* , 1–13.

[16] Tong, J., Cohnert, T., Regitnig, P. & Holzapfel, G. A. 2011 Effects of age on the elastic properties of the intraluminal thrombus and the thrombus-covered wall in abdominal aortic aneurysms: biaxial extension behaviour and material modelling. *Eur. J. Vasc. Endovasc. Surg.* **42**, 207–19.

[17] Scott, D. J. A. et al. 2011 Clot architecture is altered in abdominal aortic aneurysms and correlates with aneurysm size. *Arterioscler. Thromb. Vasc. Biol.* **31**, 3004–10.

[18] Varjú, I., Sótonyi, P., Machovich, R., Szabó, L., Tenekedjiev, K., Silva, M. M. C. G., Longstaff, C. & Kolev, K. 2011 Hindered dissolution of fibrin formed under mechanical stress. *J. Thromb. Haemost.* **9**, 979–86.

[19] Weisel, J. W. 2011 Stressed fibrin lysis. *J. Thromb. Haemost.* **9**, 977–8.

[20] Houard, X., Touat, Z., Ollivier, V., Louedec, L., Philippe, M., Sebbag, U., Meilhac, O., Rossignol, P. & Michel, J.-B. 2009 Mediators of neutrophil recruitment in human abdominal aortic aneurysms. *Cardiovasc. Res.* **82**, 532–41.

[21] Adolph, R., Vorp, D. A., Steed, D. L., Webster, M. W., Kameneva, M. V & Watkins, S. C. 1997 Cellular content and permeability of intraluminal thrombus in abdominal aortic aneurysm. *J. Vasc. Surg.* **25**, 916–26.

[22] Fontaine, V., Jacob, M.-P., Houard, X., Rossignol, P., Plissonnier, D., Angles-Cano, E. & Michel, J.-B. 2002 Involvement of the mural thrombus as a site of protease release and activation in human aortic aneurysms. *Am. J. Pathol.* **161**, 1701–10.

[23] Nackman, G. B., Karkowski, F. J., Halpern, V. J., Gaetz, H. P. & Tilson, M. D. 1997 Elastin degradation products induce adventitial angiogenesis in the Anidjar/Dobrin rat aneurysm model. *Surgery* **122**, 39–44.

[24] Valentín, A., Humphrey, J. D. & Holzapfel, G. A. 2011 A multi-layered computational model of coupled elastin degradation, vasoactive dysfunction, and collagenous stiffening in aortic aging. *Ann. Biomed. Eng.* **39**, 2027–2045.

[25] Isenberg, B. C. & Tranquillo, R. T. 2003 Long-Term Cyclic Distention Enhances the Mechanical Properties of Collagen-Based Media-Equivalents. *Ann. Biomed. Eng.* **31**, 937–949.

[26] Lillie, M. A. & Gosline, J. M. 2007 Mechanical properties of elastin along the thoracic aorta in the pig. *J. Biomech.* **40**, 2214–2221.

[27] Choke, E., Cockerill, G., Wilson, W. R. W., Sayed, S., Dawson, J., Loftus, I. & Thompson, M. M. 2005 A review of biological factors implicated in abdominal aortic aneurysm rupture. *Eur. J. Vasc. Endovasc. Surg.* **30**, 227–44.

[28] Fillinger, M. F., Marra, S. P., Raghavan, M. L. & Kennedy, F. E. 2003 Prediction of rupture risk in abdominal aortic aneurysm during observation: Wall stress versus diameter. *J. Vasc. Surg.* **37**, 724–732.

[29] Burke, A. & Fitzgerald, G. A. 2003 Oxidative stress and smoking-induced vascular injury. *Prog. Cardiovasc. Dis.* **46**, 79–90.

[30] Powell, J. T. 1998 Vascular damage from smoking: disease mechanisms at the arterial wall. *Vasc. Med.* **3**, 21–28.

[31] Mahmud, A. & Feely, J. 2003 Effect of smoking on arterial stiffness and pulse pressure amplification. *Hypertension* **41**, 183–187.

[32] Enevoldsen, M. S., Henneberg, K. A., Jensen, J. A., Lönn, L. & Humphrey, J. D. 2011 New interpretation of arterial stiffening due to cigarette smoking using a structurally motivated constitutive model. *J. Biomech.* **44**, 1209–1211.

[33] Bhak, R. H., Wininger, M., Johnson, G. R., Lederle, F. A., Messina, L. M., Ballard, D. J. & Wilson, S. E. 2015 Factors associated with small abdominal aortic aneurysm expansion rate. *JAMA Surg.* **150**, 44–50.

[34] Al-Barjas, H. S., Ariëns, R., Grant, P. & Scott, J. A. 2006 Raised plasma fibrinogen concentration in patients with abdominal aortic aneurysm. *Angiology* **57**, 607–14.

[35] van den Berkmortel, F. W. P. J., Wollersheim, H., van Langen, H., Smilde, T. J., den Arend, J. & Thien, T. 2004 Two years of smoking cessation does not reduce arterial wall thickness and stiffness. *Neth. J. Med.* **62**, 235–241.

[36] Jatoi, N. A., Jerrard-Dunne, P., Feely, J. & Mahmud, A. 2007 Impact of smoking and smoking cessation on arterial stiffness and aortic wave reflection in hypertension. *Hypertension* **49**, 981–985.

[37] Meade, T. W., Imeson, J. & Stirling, Y. 1987 Effects of changes in smoking and other characteristics on clotting factors and the risk of ischaemic heart disease. *Lancet* **330**, 986–988.

[38] Deuel, T. F., Senior, R. M., Chang, D., Griffin, G. L., Heinrikson, R. L. & Kaiser, E. T. 1981 Platelet factor 4 is chemotactic for neutrophils and monocytes. *Proc. Natl. Acad. Sci. U. S. A.* **78**, 4584–4587.

[39] Golledge, J., Muller, J., Daugherty, A. & Norman, P. 2006 Abdominal aortic aneurysm: Pathogenesis and implications for management. *Arterioscler. Thromb. Vasc. Biol.* **26**, 2605–2613.

[40] Parodi, F. E., Mao, D., Ennis, T. L., Bartoli, M. A. & Thompson, R. W. 2005 Suppression of experimental abdominal aortic aneurysms in mice by treatment with pyrrolidine dithiocarbamate, an antioxidant inhibitor of nuclear factor-kB. *J. Vasc. Surg.* **41**, 479–489.

[41] Steinmetz, E. F., Buckley, C., Shames, M. L., Ennis, T. L., Vanvickle-Chavez, S. J., Mao, D., Goeddel, L. A., Hawkins, C. J. & Thompson, R. W. 2005 Treatment with simvastatin suppresses the development of experimental abdominal aortic aneurysms in normal and hypercholesterolemic mice. *Ann. Surg.* **241**, 92–101.

[42] Lindholt, J. S., Sorensen, H. T., Michel, J. B., Thomsen, H. F. & Henneberg, E. W. 2008 Low-dose aspirin may prevent growth and later surgical repair of medium-sized abdominal aortic aneurysms. *Vasc. Endovascular Surg.* **42**, 329–34.

[43] Owens, A. P. et al. 2015 Platelet inhibitors reduce rupture in a mouse model of established abdominal aortic aneurysm. *Arterioscler. Thromb. Vasc. Biol.* **35**, 2032–2041.

[44] Lawrence, D. M., Singh, R. S., Franklin, D. P., Carey, D. J. & Elmore, J. R. 2004 Rapamycin suppresses experimental aortic aneurysm growth. *J. Vasc. Surg.* **40**, 334–338.

[45] Arnoud Meijer, C., Stijnen, T., Wasser, M. N. J. M., Hamming, J. F., Van Bockel, J. H. & Lindeman, J. H. N. 2013 Doxycycline for stabilization of abdominal aortic aneurysms: A randomized trial. *Ann. Intern. Med.* **159**, 815–823.

[46] Brown, P. M., Zelt, D. T. & Sobolev, B. 2003 The risk of rupture in untreated aneurysms: The impact of size, gender, and expansion rate. *J. Vasc. Surg.* **37**, 280–284.

[47] Ahimastos, A. A., Formosa, M., Dart, A. M. & Kingwell, B. A. 2003 Gender differences in large artery stiffness pre- and post puberty. *J. Clin. Endocrinol. Metab.* **88**, 5375–5380.

[48] Celermajer, D. S., Sorensen, K. E., Spiegelhalter, D. J., Georgakopoulos, D., Robinson, J. & Deanfield, J. E. 1994 Aging is associated with endothelial dysfunction in healthy men years before the age-related decline in women. *J. Am. Coll. Cardiol.* **24**, 471–6.

[49] Blanchard, J. F., Armenian, H. K. & Friesen, P. P. 2000 Risk factors for abdominal aortic aneurysm: results of a case-control study. *Am. J. Epidemiol.* **151**, 575–583.

[50] Vande Gee″st, J. P., Sacks, M. S. & Vorp, D. A. 2006 The effects of aneurysm on the biaxial mechanical behavior of human abdominal aorta. *J. Biomech.* **39**, 1324–34.

[51] Tong, J., Schriefl, A. J., Cohnert, T. & Holzapfel, G. A. 2013 Gender differences in biomechanical properties, thrombus age, mass fraction and clinical factors of abdominal aortic aneurysms. *Eur. J. Vasc. Endovasc. Surg.* **45**, 364–72.

[52] Brown, L. C. & Powell, J. T. 1999 Risk factors for aneurysm rupture in patients kept under ultrasound surveillance. *Ann. Surg.* **230**, 289–297.

[53] O'Rourke, M. J., McCullough, J. P. & Kelly, S. 2012 An Investigation of the relationship between hemodynamics and thrombus deposition within patient-specific models of abdominal aortic aneurysm. *Proc. Inst. Mech. Eng. Part H J. Eng. Med.* **226**, 548–564.

[54] Chobanian, A. V. et al. 2003 Seventh report of the Joint National Committee on Prevention, Detection, Evaluation, and Treatment of High Blood Pressure. *Hypertension* **42**, 1206–1252.

[55] Parr, A., McCann, M., Bradshaw, B., Shahzad, A., Buttner, P. & Golledge, J. 2011 Thrombus volume is associated with cardiovascular events and aneurysm growth in patients who have abdominal aortic aneurysms. *J. Vasc. Surg.* **53**, 28–35.

[56] Golledge, J., Iyer, V., Jenkins, J., Bradshaw, B., Cronin, O. & Walker, P. J. 2014 Thrombus volume is similar in patients with ruptured and intact abdominal aortic aneurysms. *J. Vasc. Surg.* **59**, 315–20.

[57] Krievins, D., Thora, S. & Zarins, C. K. 2015 Gigantic 25-cm abdominal aortic aneurysm. *J. Vasc. Surg.* **61**, 1067.

[58] Humphrey, J. D. & Taylor, C. A. 2008 Intracranial and abdominal aortic aneurysms: similarities, differences and need for a new class of computational models. *Annu. Rev. Biomed. Eng.* **10**, 221–246.